Environmental Science & Technology

pubs.acs.org/est

Article

pH Dependence of Phosphorus Speciation and Transport in Flow-Electrode Capacitive Deionization

Yanhong Bian, Xi Chen, and Zhiyong Jason Ren*

Cite This: *Environ. Sci. Technol.* 2020, 54, 9116–9123

Read Online

ACCESS | Metrics & More | Article Recommendations | Supporting Information

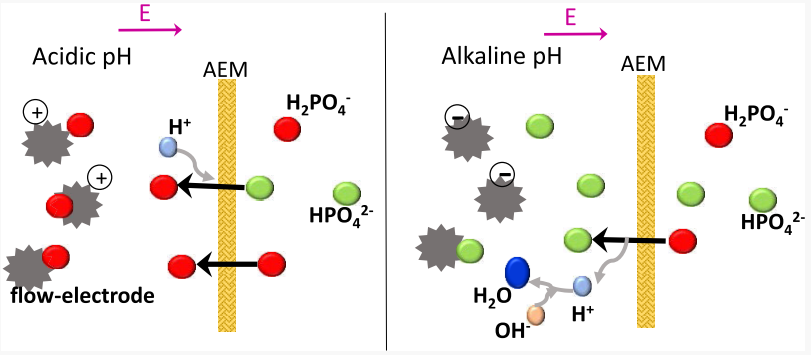

ABSTRACT: Electrochemical processes such as capacitive deionization have shown great promise for salt removal and nutrient recovery, but their effectiveness on phosphate removal was lower than other charged ions. This study hypothesized that the speciation and transport behaviors of phosphate ions are highly influenced by electrolyte pH, and it used experimental and modeling approaches to elucidate such impacts in flow-electrode capacitive deionization (FCDI) cells. Phosphate removal was investigated in either constant current (CC) or constant voltage (CV) charging mode with pH ranged from 5 to 9 in the feed solution. Results showed that the average P removal rate increased from 20.8 (CC mode) and 16.8 mg/min (CV mode) at pH 9 to 38.3 (CC mode) and 34.3 mg/min (CV mode) at pH 5 (84−104% in improvement), respectively. Correspondingly, the energy consumption reduced from 1.04 kWh/kg P at pH 9 to 0.59 kWh/kg P at pH 5 (42.9−56.1% in saving). Such benefits were attributed to the shift in dominant P-species from HPO_4^{2-} to $H_2PO_4^-$. Conversely, high-electrolyte pH (pH = 11) for flow-electrode led to ∼74.8% higher phosphate recovery during discharge compared with pH 5, which was associated with the higher distribution of phosphate ions in the electrolyte versus on the flow-electrodes due to surface charge change. These results improved our understanding in ion distribution and migration and indicate that solution pH is critical for operating FCDI reactors. It shed lights on the best practices on electrochemical phosphate removal and recovery.

INTRODUCTION

Phosphorus (P) is an essential nutrient for life, but it is also a major pollutant that leads to eutrophication.[1] Phosphorus is primarily obtained from mineral phosphorus rocks that are concentrated in a limited number of countries, so the recovery of P from waste streams carries significant impacts on economic development and national security.[2] Globally, approximately 1.3 Mt P/year is treated in municipal wastewater treatment plants (WWTPs), but current P-removal processes have limited capability of recovery.[3]

Phosphorus in wastewater can be removed using physicochemical and/or biological treatment processes. Chemical P removal involves the addition of calcium, iron, or aluminum salts to bind and precipitate P in the wastewater and generate solid residuals.[4−6] Chemical precipitation is known for high efficiency, but the chemically bonded P is difficult to be utilized again by organisms.[7,8] Enhanced biological P removal (EBPR) has been widely implemented in large wastewater treatment plants. By alternating anaerobic−aerobic operational conditions, polyphosphate-accumulating organisms (PAOs) can directly take up phosphate from wastewater and synthesize polyphosphate containing biomass.[9,10] EBPR has the advantage of zero chemical consumption with P accumulated in biosolids, but it has faced challenges to remove P to μg/L level to meet more stringent discharge regulations. In addition, EBPR requires skilled operators for process control or the performance can fluctuate significantly. This poses challenges for EBPR's application in small-scale systems, which lack the resources of skilled operators and monitoring systems.

Received: March 24, 2020
Revised: June 24, 2020
Accepted: June 25, 2020
Published: June 25, 2020

https://dx.doi.org/10.1021/acs.est.0c01836
Environ. Sci. Technol. 2020, 54, 9116–9123

Electrochemical processes including capacitive deionization (CDI) recently emerged as new approaches for P recovery especially as modular systems suitable for distributed applications.[11−14] These systems take advantage of an electrical field to remove charged ion species including phosphate from wastewater, brackish water, and other impaired water resources and store them on electrodes followed by discharging ions into concentrate for recovery.[15−18] Among different CDI configurations, flow-electrode capacitive deionization (FCDI) showed a unique advantage on continuous charge−discharge operation using suspended carbon electrodes, which can be regenerated continuously during discharge.[19−22] There are two commonly used operation modes for FCDI in terms of fluid flow, isolated closed cycle (ICC) mode, and short-circuited closed cycle (SCC) mode.[23,24] SCC mode was reported more energy efficient because it enables simultaneous regeneration via the mixing of the anode and cathode flow-electrodes in an external reservoir.[25] In contrast, the anode and cathode flow-electrodes in the ICC mode are individually recycled and the regeneration needs an additional discharge stage. Phosphate can be recovered by either concentrated in a flow-electrode solution or discharged to the middle chamber as an enriched nutrients solution. However, compared with other charged ions, such as salts and nitrogen species, the removal efficiency of phosphate in CDI/FCDI has been much lower. For example, Ge et al. found high removals of salts (78%) and NH_4^+ (61%) in CDI under an 1.2 V applied voltage, while the removal of phosphate was only 46%.[26] Another study by Jiang et al. reported similar observations, where the preferential electrosorption sequence in membrane capacitive deionization (MCDI) was Cl^- > SO_4^{2-} > P when the initial ion concentration order was Cl^- (1.9 mM) > P (0.4 mM) > SO_4^{2-} (0.32 mM).[27] Previous explanations were that phosphate concentration was lower and phosphate hydrated radius was larger.[26,28] These considerations overlooked a fundamental aspect that phosphate speciation in different water conditions may have big impacts on ion transfer and sorption/desorption. The dominant phosphate species in the feed solution and flow-electrode varies with pH in compliance with following reversible reactions,[29] as shown in Figure S1

$$H_3PO_4 \rightleftharpoons H^+ + H_2PO_4^- \quad pK_{a1} = 2.148 \tag{1}$$

$$H_2PO_4^- \rightleftharpoons H^+ + HPO_4^{2-} \quad pK_{a2} = 7.198 \tag{2}$$

$$HPO_4^{2-} \rightleftharpoons H^+ + PO_4^{3-} \quad pK_{a3} = 12.375 \tag{3}$$

Previous studies by Zhang et al. demonstrated that by utilizing pH gradient in the cathode, NH_4^+ recovery could be selectively increased in FCDI via membrane separation.[30,31] Typical wastewaters have a pH range from 6 to 8, and recent studies also showed that the increased feed solution pH could reduce phosphate removal due to the changes in dominant P species and their corresponding charges.[32,33] However, the mechanisms of pH dependence of P species transfer in the whole FCDI cell are not well understood, especially when considering phosphate has strong buffering capacity and the FCDI anode pH could decrease to lower than 5 during electrosorption in the ICC mode.[34]

In this study, we characterized pH dependence of phosphate speciation and transport in flow-electrode capacitive deionization and discussed the strategies to improve phosphate removal and recovery efficiency in different conditions. We investigated the P removal/recovery performance of FCDI in the ICC mode. Although the SCC is more energy efficient, the OH^- released from the cathode chamber can affect the pH of the flow-electrode and it will be difficult to maintain a desired pH value in the anode.[25] Constant current (CC) and constant voltage (CV) charging modes were applied and compared to understand phosphate removal and energy consumption in FCDI, and preliminary fitting using Nernst−Planck equation was carried out.

MATERIALS AND METHODS

FCDI Characteristics. Lab scale FCDI cells were constructed and used for phosphate transfer studies, which has been described in our previous work.[11] Briefly, two graphite plate current collectors/membranes/spacer assemblies were compacted firmly by two end plates. Graphite plate current collectors with a curved channel (2 mm deep and 2 mm wide) was also used as flow channels for flow-electrodes. A nylon spacer between a pair of cation and anion exchange membranes (CEM and AEM, Membrane International) was used as a feed solution channel.[35] Each FCDI had a total volume of feed solution of 4.4 mL and an effective membrane surface area of 11.7 cm^2.

Experimental Setup. The FCDI cell was operated with single-pass mode, as shown in Figure S2. The system consisted of a pair of feed/effluent tank, a peristaltic pump (Cole-Parmer), an FCDI cell, and a conductivity meter (HQ440d, HACH). A series of experiments were conducted to investigate the phosphate speciation changes and transfer behaviors under different solution pH as well as during the changes of pH in flow-electrodes electrolyte. The initial phosphate concentration was set as 500 mg P/L (16 mM) to avoid phosphate transfer limitation caused by the low concentration in the feed solution. All of the flow-electrodes were prepared by mixing of 10 wt % of activated carbon with 90 wt % of DI water, and the conductivity of the flow-electrodes was 120 ± 15 μS/cm. The total mass of each anode and cathode was 60 g. The flow rates of both feed solution and flow-electrode were set as 9.5 mL/min. Constant current (CC) and constant voltage (CV) charging modes were applied to investigate the effects of the feed solution on phosphate removal. During adsorption, a constant charging voltage of 1.2 V was applied in the CV mode, while a constant electric current of 12 mA applied in the CC mode by a DC power source. The initial pH of the feed solution was tested from 5 to 9 by adjusting the initial ratio of NaH_2PO_4 and Na_2HPO_4. The conductivities of the feed solution were 1340 ± 10 μS/cm at pH 5, 1780 ± 13 μS/cm at pH 7, and 2600 ± 16 μS/cm at pH 9, respectively. Traditional flow-electrodes of FCDI were prepared using neutral electrolyte, which generally led to variable anode pH during charging and resulted in low pH as a result. To better understand the effects of anolyte pH on P transport in FCDI in a broader pH spectrum, the initial pH of flow-electrodes was tested from 3 to 11 adjusted using HCl or NaOH and the pH of the feed solution was set as 7. A constant 12 mA was applied for 2 h during adsorption, while a reverse 18 mA was applied for 1 h during desorption. The effluent from FCDI outlet was sampled every 10 min for both adsorption and desorption. The flow-electrodes of both anode and cathode were sampled every 30 min during adsorption and 20 min during desorption for further analysis.

Analysis and Calculations. The current and voltage across the FCDI cell were recorded using a data acquisition system at an interval of 30 s. The conductivity of the feed

https://dx.doi.org/10.1021/acs.est.0c01836
Environ. Sci. Technol. 2020, 54, 9116−9123

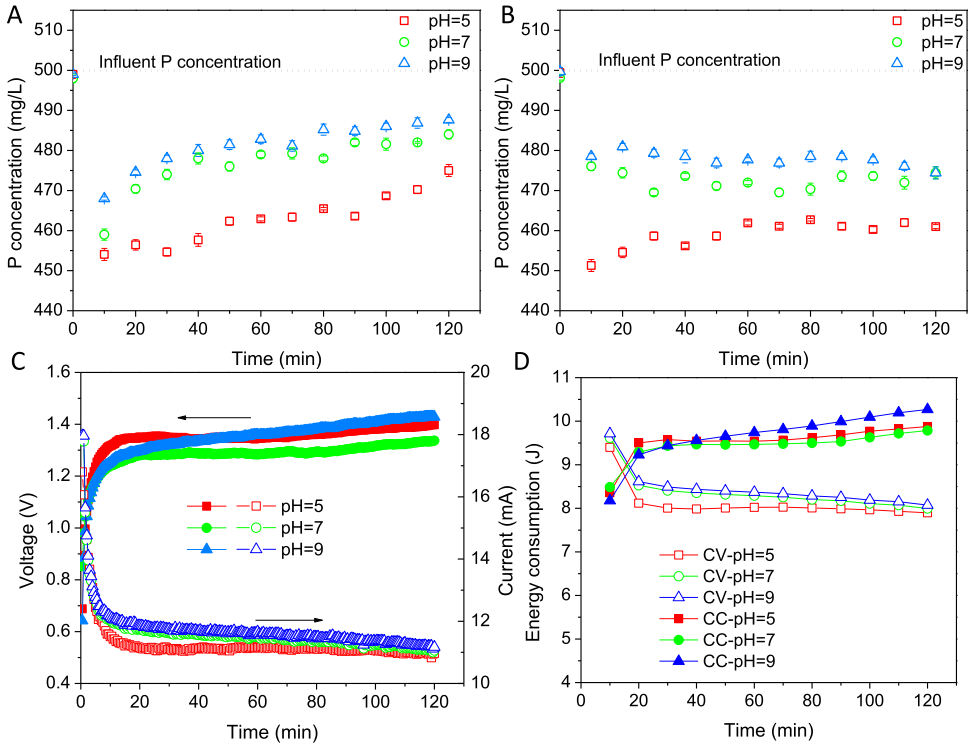

Figure 1. Overall P-concentration profiles under different feed solution pHs in (A) constant voltage (CV) mode and (B) constant current (CC) mode during charging stages for 2 h. (C) Current and voltage profiles of CV and CC charging modes. (D) Energy consumption of every 10 min operated in CC and CV charging modes.

solution was measured in real time with an interval of 30 s (HQ440d, HACH). The pH of the water sample from FCDI effluent and electrode sample from anode and cathode were measured using a pH meter (Orion Star A216, ThermoFisher). The total phosphate concentration as P was measured using HACH standard tests (TNT 846, TNT 844) with a spectrophotometer (HACH, Loveland). The zeta potential of flow-electrode was measured to investigate the influence of pH on surface charge of activated carbon particle (Zeta-check, Colloid Metrix).[36] To further evaluate the performance, the amount of phosphorus removal ($T_{removal,}$ mg), the phosphorus removal rate (R_P, mg/min), the current efficiency of P removal (%), and the normalized energy consumption of phosphorus removal (kWh/kg P) were determined as follows

$$T_{removal} = \int_0^t (C_{0,P} - C_{t,P}) Q \, dt \tag{4}$$

$$R_P = \frac{\int_0^t (C_{0,P} - C_{t,P}) Q \, dt}{\int_0^t dt} \tag{5}$$

$$\text{current efficiency} = \frac{\sum \int_0^t n_x F Q (C_{0,x} - C_{t,x}) dt}{M \int_0^t I dt} \tag{6}$$

$$EC = \frac{\int VI dt \times 3.6}{\int (C_{0,P} - C_{t,P}) Q \, dt} \tag{7}$$

where $C_{0,P}$ and $C_{t,P}$ were phosphorus concentration (mg/L) in initial and effluent solutions, respectively; $C_{0,x}$ and $C_{t,x}$ were phosphate (H_2PO^{4-}, HPO_4^{2-}, PO_4^{3-}) concentrations in initial and effluent solutions (mg P/L), respectively; n_x was the ion charge (1 for $H_2PO_4^-$, 2 for HPO_4^{2-} and 3 for PO_4^{3-}); F was the Faraday constant (96 485 C/mol); M was the molar mass of phosphorus (g/mol); Q was the flow rate (L/s); t was the charging time (s); and V and I were applied voltage (V) and current (A), respectively.

Phosphate Transport Model when Considering Solution pH. During the charging stage of the FCDI operation, phosphate ions are considered to be removed after migrating across the anion exchange membrane from the spacer channel. Since the phosphate ion transport in the spacer channel of FCDI is a combination of diffusion and electromigration, Nernst−Planck equation can be used to describe phosphate transport, which is shown in the following equation8[37]

$$J_i = -\frac{D_i}{\tau_s}\left(\frac{dC_i}{dx} + z_i C_i \frac{d\phi}{dx}\right) \tag{8}$$

where J_i is the flux of phosphate ion species ($H_2PO_4^-$, HPO_4^{2-}, PO_4^{3-}), τ_s is the tortuosity of the spacer, D_i, C_i, and z_i are the diffusion coefficient, concentration, and charge of phosphate species, respectively, and $\frac{d\phi}{dx}$ is the dimensionless potential gradient in the spacer channel. As FCDI has a complete mix flow pattern, the ions transport caused by concentration gradient is considered negligible. Since the main phosphate ions species are $H_2PO_4^-$ and HPO_4^{2-} at pH 5−9, the flux ratio of $H_2PO_4^-$ to HPO_4^{2-} can simplify to

$$\frac{J_{H_2PO_4^-}}{J_{HPO_4^{2-}}} = \frac{D_{H_2PO_4^-}}{D_{HPO_4^{2-}}} \cdot \frac{z_{H_2PO_4^-}}{z_{HPO_4^{2-}}} \cdot \frac{C_{H_2PO_4^-}}{C_{HPO_4^{2-}}} \tag{9}$$

The diffusion coefficients of $H_2PO_4^-$ and HPO_4^{2-} are 8.79×10^{-10} and 4.39×10^{-10} m^2/s, respectively.[32] The concentration

https://dx.doi.org/10.1021/acs.est.0c01836
Environ. Sci. Technol. 2020, 54, 9116−9123

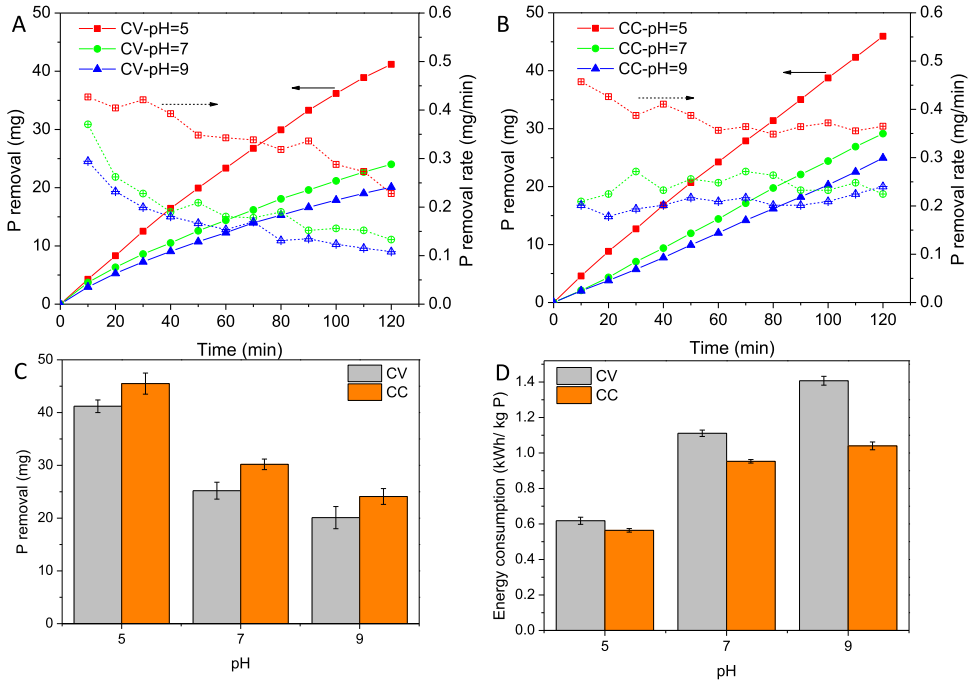

Figure 2. Effects of pH on (A) time-course P removal and rates in the CV mode, (B) time-course P removal and rates in the CC mode, (C) total amount of P removal in 2 h operation, and (D) energy consumption per kg of P removed during the charging stage.

ratio of phosphate ion species depends on the pH of the feed solution based on the revisable reaction eq 2

$$\frac{C_{H_2PO_4^-}}{C_{HPO_4^{2-}}} = \frac{C_{H+}}{K_{a2}} = 10^{pK_{a2}-pH} \quad (10)$$

where K_{a2} and pK_{a2} are equilibrium constant of reaction 2 and its negative log value (pK_{a2} = 7.198), respectively.

RESULTS AND DISCUSSION

Overall Phosphate Transport and Energy Consumption under Different Feed Solution pHs. Figure 1A,B shows the overall variations of P concentration in the effluent during electrosorption in CC and CV charging modes with different pH ranges from 5 to 9. The effluent P concentration changes with time, and the ions removal behavior changes with different charging modes. Figure 1A shows that the P concentration in the effluent dropped rapidly in the first 10 min when applied a constant voltage. Then, it slowly increased during the charging stage, which corresponded with the reduced current over the time course. In contrast, the effluent P concentration decreased and then remained steady in CC operation mode. Since the ion transfer kinetic rate was roughly proportional to the charging current, ions were also removed in a constant rate during CC charging. Figure 1C shows that both current and voltage in the CC mode were stable after polarization at the beginning of charging. The reason why current or voltage was stable was that the conductivity of the feed solution passing through the FCDI spacer remained the same in the single-pass operation mode. It is noted that the phosphate effluent concentration in the CC mode was lower than that of in the CV mode for the same pH condition, which was caused by the higher current (12 mA) applied in CC mode compared with that in the CV mode (averaged current 11.26–11.72 mA). Figure 1D shows the energy consumption of FCDI in every 10 mins' operation, and it can be seen that lower energy was applied for the CV mode (averaged energy consumption 8.11–8.44 J) compared with that for the CC mode (averaged energy consumption 9.44–9.67 J). The effluent P concentration was lower at lower pH for both CC and CV modes, as shown in Figure 1A,B, which suggests that lower pH resulted in higher P removal in FCDI.

Figure 2 summarizes the phosphate removal (in terms of P) and energy consumption under CC or CV modes at different pH conditions. As shown in Figure 2A,B, the phosphate removal rates for both CC and CV modes increased when the feed solution pH decreased. When the initial feed solution pH decreased from 9 to 5, the phosphate removal rates with CV and CC modes increased 45.0–149.0 and 51.9–139.1%, respectively. Correspondingly, the final phosphate removal amounts in 2 h operation under CV and CC modes increased from 20.1 to 41.2 mg P (105% improvement) and from 25.0 to 45.9 mg P (83.6% improvement), respectively (Figure 2C). These results indicate that the phosphate removal was more effective at lower pH, which is consistent to observations in previous studies.[13,32,38] The enhanced phosphate removal at lower pH 5 compared with pH 9 is caused by the variation of P species ($H_2PO_4^-$ and HPO_4^{2-}) present in the solution, which will further discussed in the modeling session. Figure S1 shows the phosphate speciation diagram from pH 0 to 14. It shows that $H_2PO_4^-$ dominates at pH 5 and the fraction of $H_2PO_4^-$ gradually decreases with increasing pH, and HPO_4^{2-} becomes dominant phosphate specie when the pH reaches 9.0. During the operation, it was observed that the pH of effluent only changed slightly (less than 1 unit) for both CC and CV modes (Figure S3), which means that the dominant phosphate specie in the spacer channel in FCDI remained the same during the whole charging stage in each operation condition (i.e., $H_2PO_4^-$ in pH 5 and HPO_4^{2-} in pH 9 in respective batches). While pH fluctuations were observed during electrosorption in previous studies,[39] the reason why the effluent pH only changed slightly in this study is that the buffer capacity of the electrolytes used

https://dx.doi.org/10.1021/acs.est.0c01836
Environ. Sci. Technol. 2020, 54, 9116–9123

here reduced the range of variation. After 2 h operation, the total phosphate removal in the CV mode was 10.3−19.4% lower than that of the CC mode for all of the three feed solution pH conditions (Figure 2C). The main reason for better phosphate removal of the CC mode than that of the CV mode is related to the higher current setting discussed above.

Figure 2D shows the energy consumption for phosphate removal in CV and CC modes. It can be observed that energy consumptions in the CC mode are ∼5−25% lower than that in the CV mode, which could be attributed to the lower voltage at the beginning of the charging stage and different setting levels of the two charging modes. Here, the energy consumption of phosphate removal increased as pH increased. For CC mode charged FCDI, the energy consumption increased from 0.594 kWh/kg P at pH 5 to 1.04 kWh/kg P at pH 9, representing a 75.1% increase. As in the CV mode, the energy consumption increased from 0.618 to 1.407 kWh/kg P or 127.7%. The energy used in these operations were lower to our previous studies that used in FCDI/CDI because much higher initial concentration of phosphorus was applied in this study.[11,26] The findings provide new insights that by controlling the feed solution at lower pH, energy efficiency can be improved for phosphorus removal. In contrast to energy consumption normalized by phosphorus mass, results of current efficiency (Table S1) showed no significant difference under different pHs in both CC (71−77%) and CV modes (67−75%). Similar charge efficiencies were observed for CC and CV charging modes. This suggests that almost the same amount of charges were used for phosphate ions removal. The discrepancy in energy consumption and P removal rate were attributed to different charge numbers of each dominant charge carrier (i.e., 1 for $H_2PO_4^-$ and 2 for HPO_4^{2-}) at different pHs. The CC mode operation is preferred as it carries the advantage in easy tuning of the effluent concentration via current control, which could also result in relative constant phosphate effluent concentration.[40] Herein, the CC charging mode was used to investigate the phosphate transfer behavior in the following experiments.

Phosphate Speciation and Transport Described by Nernst−Planck Equation. When the feed solution pH was 5−9, the dominate phosphate ions are $H_2PO_4^-$ and HPO_4^{2-}. The flux ratio of $H_2PO_4^-$ and HPO_4^{2-} also depends on the pH of the feed solution in FCDI. The relationship between the flux ratio and feed solution pH is described in Figure 3, in which solid curves are simulated results and empty symbols are actual experimental data. For all experimental data with CC and CV charging modes discussed above, the flux ratios of $H_2PO_4^-$ and HPO_4^- were calculated based on the phosphorus removal and their corresponding pH values. The simulated results from Nernst−Planck equation fit the experimental results very well (Figure 3), proving the validity of the model in describing phosphate transfer behavior in FCDI spacer channel. Figure 3 shows that pH has a significant influence on phosphate species transport, and the dominant ions transport at pH 5 and 9 are $H_2PO_4^-$ and HPO_4^{2-}, respectively. Since dihydrogen phosphate $H_2PO_4^-$ carries one charge and hydrogen phosphate HPO_4^{2-} carries two charges, more phosphorus was removed from spacer channel at pH 5 in the form of $H_2PO_4^-$ than at pH 9 in the form of HPO_4^- with the same amount of charge transfer in the cell. As a result, adjusting the feed solution pH to a lower value should enhance phosphate removal in FCDI. The simulated results well aligned with the experimental data, and it demonstrates the ratio between dominant species in

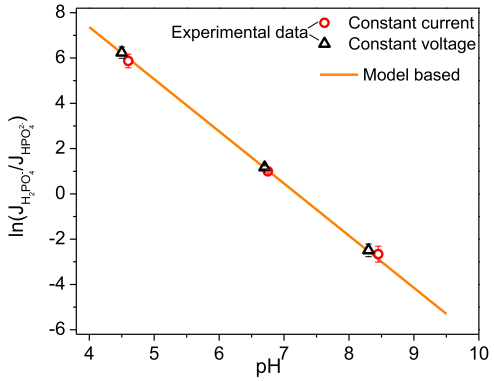

Figure 3. Ratio between fluxes of $H_2PO_4^-$ and HPO_4^{2-} ($N_{H_2PO_4^-}/N_{HPO_4^{2-}}$) as a function of feed solution pH in FCDI. The solid line is generated using the Nernst−Planck equation, while the empty symbols are experimental data with the error bars representing standard deviations.

different pHs as well as their projected removals under either the CC or CV mode. It should be noted that the simplified model is only applicable to describe phosphate transport in the spacer channel, and further studies are needed to simulate the phosphorus adsorption in the flow-electrode. While only phosphate anions are considered in this study, further optimization is needed to describe real wastewater operation with multi-ions and complex ions interactions.

Phosphate Distribution under Different Flow Electrolyte pHs. Figure 4 shows the phosphate removal and recovery in FCDI with different electrolyte pHs of flow-electrodes. Typical electrosorption/desorption cycles in a single-pass mode are observed in Figure 4A, in which a lower concentration effluent was obtained during the charging stage and a higher concentration effluent during the discharging stage. Phosphate removal during the charging stage for electrolyte with different flow electrolyte pHs showed no significant differences. The energy consumptions of P removal were also similar with different electrolyte pHs (Table S2). The removal performance was slightly higher for higher pH, which may be caused by the relative higher conductivity of the flow-electrodes due to pH adjustment. In contrast, Figure 4B shows that the phosphate ions distribution after 2 h charging is totally different. A pH-dependent ion distribution was observed when electrolyte pH ranges from 3 to 11, in which higher percentages of phosphate were located in the anode electrolyte for higher pH. For example, only 7.1% ions presented in the electrolyte when electrolyte pH was 3, while about half of the removed phosphorus ions (45%) presented in the electrolyte at pH 11. The discrepancy of phosphate distribution is hypothesized associated with the changes of surface charge of activated carbon particles at different pHs. The zeta potentials of flow-electrodes in electrolyte at different pHs were measured, and the results are shown in Figure S4. The carbon surface is positively charged when the electrolyte pH is lower than 5 and is negatively charged when the pH is higher than 7. Although the zeta potential values vary based on different AC materials, a zeta potential versus pH curve of the materials is generally higher or positive at low pH and lower or negative at high pH.[41−44] Since phosphate species are negatively charged anions in the aqueous phase, it is expected that more phosphate ions are dissolved in the electrolyte at high pH than at low pH after migrating across the anion

https://dx.doi.org/10.1021/acs.est.0c01836
Environ. Sci. Technol. 2020, 54, 9116−9123

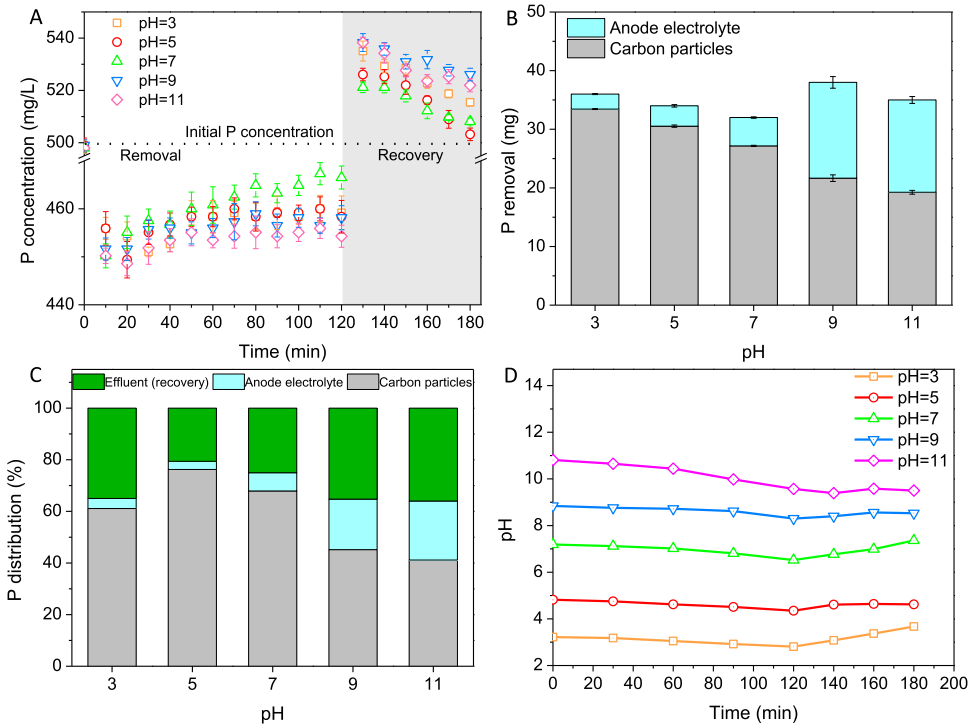

Figure 4. Phosphate distribution under different flow electrolyte pHs. (A) Effluent P concentration during charging and discharging stages. (B) P removal and distribution. (C) P recovery and distribution after discharging stage. (D) Variations of pH of anode electrolyte during charging and discharging stage.

exchange membrane as long as they are in the form of anions. Although the zeta potential values of AC were negative when pH > 7, there were still a large amount of phosphorus located on the carbon particles (Figure 4B). The phosphate ions could be electrostatically adsorbed on AC to neutralize the positive charge provided by the external electric field. Another possible reason was the nonelectrostatical phosphorus adsorption occurred by physicochemical mechanisms, which was reported in previous studies.[25,26] It should be noted that when the pH of anode electrolyte is lower than 2, more than 58.5% of P presents as uncharged H_3PO_4 (Figure S1). After migrating across the membrane, most of phosphate ions (either $H_2PO_4^-$ or HPO_4^-) will be converted to H_3PO_4 and dissolve in the electrolyte in such conditions.

When the direction of electric field was reversed for discharging, the phosphate ions adsorbed on the activated carbon particles or dissolved in the electrolyte were transferred to the middle chamber of FCDI to enable phosphate recovery in a form of concentrate. The recovery performance of phosphate at different initial pHs of flow-electrode electrolyte after 1 h discharging is shown in Figure 4C. The phosphate recovery efficiency increased from 20.6 to 36% when the electrolyte pH increased from 5 to 11. A possible explanation here relates to different phosphate distributions after the charging stage. Since a significant amount of phosphate ions were dissolved in the flow-electrode electrolyte at pH 11, it is much easier for the phosphate in the electrolyte to migrate across the anion exchange membrane than those phosphate ions adsorbed on the surface of activated carbon particles. It should be noted that a higher recovery efficiency of 34% was also obtained when the pH was 3. Since most of the phosphate removed from the middle chamber (~92.9%) were adsorbed on carbon particles at pH 3 (Figure 4B), the main recovered phosphate at pH 3 should be from the desorption of phosphate from activated carbon. Although phosphate recovery efficiency can be enhanced by electrolyte pH adjustment, Figure 4C shows the recovery is still low. Previous studies have reported similar findings and explained nonelectrostatic adsorption could be a main cause. To further improve the phosphate recovery efficiency, longer discharging time and/or higher discharging voltage have been demonstrated effective.[11,26]

Figure 4D shows the pH changes of the anode electrolyte during charging and discharging stages. No significant pH drop was found in the anode during charging compared with previous FCDI studies, which was believed caused by Faradic reactions and electrodialytic process.[34,45] The relative stable pH of flow-electrodes was related to the strong buffer capacity of phosphate. However, the pH drop was much more obvious (~1.3) at pH 11 compared with that of the acidic environment at pH 3 (~0.4). This is determined by phosphate distribution after the charging stage shown in Figure 2B. Since ~45% of phosphate ions removed from the feed solution were dissolved in the electrolyte at pH 11, H^+ release caused by phosphate transformation from $H_2PO_4^-$ to HPO_4^- could result in higher pH drop in the anode. While phosphate transformation from HPO_4^- to $H_2PO_4^-$ at pH 3 consumed H^+, which caused minor pH drop in the anode.

Implications. Research in traditional CDI or FCDI reported pH changes in both the feed solution and inside the anode electrode.[46−48] Such pH variations change phosphate speciation and ion transport behaviors, which impacts phosphorus removal and recovery. This work used experimental and modeling approaches to elucidate the speciation and transport behaviors of phosphate ions in FCDI and found that the removal and recovery were largely dependent on the initial pH of the feed solution or the pH of the electrolyte. When changing the feed solution pH from 9 to 5, phosphate removal in 2 h operation increased 83.6−105%

https://dx.doi.org/10.1021/acs.est.0c01836
Environ. Sci. Technol. 2020, 54, 9116−9123

with different charging modes. When changing the pH of flow-electrode, the distribution of removed phosphate was largely dependent on the pH as well. Approximately 45% of the removed phosphate ions were dissolved in the aqueous solution of the flow-electrode at pH 11, while most (92.9%) of the phosphate ions were adsorbed on the carbon particles at pH 3. This difference was caused by the change of surface charge of activated carbon at different pHs.

Such findings indicate that tuning pH can greatly influence the phosphate removal and recovery in FCDI. Low pH operation in the feed solution is favorable as it facilitates phosphate removal as long as the dominated specie is in the form of anion (not H_3PO_4), while high anode pH is preferred to enable higher phosphate discharge and recovery. For example, the P-removal efficiency was improved by 50.7% in the CC mode and by 63.5% for the CV mode, respectively, when the pH was simply adjusted from 7 to 5. pH adjustment is a simple operation that has been widely applied in industrial wastewater treatment, but it does increase operational cost and requires neutralization before discharge. Cost−benefit analysis and environmental impacts assessment will be needed in future studies to quantify the benefits and practicality. ICC operation mode was applied to maintain the electrolyte pH at desired levels. However, combining the pH adjusting method with ICC mode might not be optimal and the P removal/recovery performance could be further improved by optimizing operation modes. In addition, the P transport in FCDI treating actual wastewater will be more complex due to the existence of other common ions (e.g., Na^+, Cl^-, NO_3^-, SO_4^{2-}, etc.), and the P concentration is relatively low especially in municipal wastewater. These factors will impact the actual removal and recovery of phosphate in application conditions, and the insights obtained from this fundamental study can help guide operations to improve the performance. Further studies should consider these actual parameters and carry out experiments with practical considerations to evaluate the technological and economic feasibility of the technology.

■ ASSOCIATED CONTENT

Supporting Information

The Supporting Information is available free of charge at https://pubs.acs.org/doi/10.1021/acs.est.0c01836.

Speciation diagram of P species from pH 0 to 14 (initial TOT_P = 16 mmol); schematic diagram of the single-pass FCDI; variation of effluent pH under different initial feed solution pH values from 5 to 9 in the CV or CC mode during charging stages; zeta potential of activated carbon at different pHs; current efficiency of P removal with different feed solution pHs in different charging modes; energy consumption of P removal with different electrolyte pHs during the charging stage (feed solution pH = 7); current efficiency calculation (PDF)

■ AUTHOR INFORMATION

Corresponding Author

Zhiyong Jason Ren − *Department of Civil and Environmental Engineering and the Andlinger Center for Energy and the Environment, Princeton University, Princeton, New Jersey 08544, United States;* orcid.org/0000-0001-7606-0331; Phone: +1 (609) 258-7580; Email: zjren@princeton.edu

Authors

Yanhong Bian − *Department of Civil and Environmental Engineering and the Andlinger Center for Energy and the Environment, Princeton University, Princeton, New Jersey 08544, United States*

Xi Chen − *Department of Civil and Environmental Engineering and the Andlinger Center for Energy and the Environment, Princeton University, Princeton, New Jersey 08544, United States;* orcid.org/0000-0003-2360-2672

Complete contact information is available at: https://pubs.acs.org/10.1021/acs.est.0c01836

Notes

The authors declare no competing financial interest.

■ ACKNOWLEDGMENTS

This work was supported by the National Science Foundation under award CEBT-1704991 and the Andlinger Center for Energy and the Environment at Princeton University.

■ REFERENCES

(1) Carpenter, S. R. Phosphorus control is critical to mitigating eutrophication. *Proc. Natl. Acad. Sci. U.S.A.* **2008**, *105*, 11039−11040.

(2) Cordell, D.; Drangert, J.-O.; White, S. The story of phosphorus: global food security and food for thought. *Global Environ. Change* **2009**, *19*, 292−305.

(3) Van Vuuren, D. P.; Bouwman, A. F.; Beusen, A. H. Phosphorus demand for the 1970−2100 period: a scenario analysis of resource depletion. *Global Environ. Change* **2010**, *20*, 428−439.

(4) Daneshgar, S.; Callegari, A.; Capodaglio, A. G.; Vaccari, D. The potential phosphorus crisis: resource conservation and possible escape technologies: a review. *Resources* **2018**, *7*, 37.

(5) Yeoman, S.; Stephenson, T.; Lester, J.; Perry, R. The removal of phosphorus during wastewater treatment: a review. *Environ. Pollut.* **1988**, *49*, 183−233.

(6) Lin, L.; Li, R.-h.; Yang, Z.-y.; Li, X.-y. Effect of coagulant on acidogenic fermentation of sludge from enhanced primary sedimentation for resource recovery: comparison between FeCl3 and PACl. *Chem. Eng. J.* **2017**, *325*, 681−689.

(7) Krogstad, T.; Sogn, T. A.; Asdal, Å.; Sæbø, A. Influence of chemically and biologically stabilized sewage sludge on plant-available phosphorous in soil. *Ecol. Eng.* **2005**, *25*, 51−60.

(8) Samie, I.; Römer, W. Phosphorus Availability to Maize Plants from Sewage Sludge Treated with Fe Compounds. In *Plant Nutrition*; Springer, 2001; pp 846−847.

(9) Zhang, H.-L.; Fang, W.; Wang, Y.-P.; Sheng, G.-P.; Zeng, R. J.; Li, W.-W.; Yu, H.-Q. Phosphorus removal in an enhanced biological phosphorus removal process: roles of extracellular polymeric substances. *Environ. Sci. Technol.* **2013**, *47*, 11482−11489.

(10) Tarayre, C.; De Clercq, L.; Charlier, R.; Michels, E.; Meers, E.; Camargo-Valero, M.; Delvigne, F. New perspectives for the design of sustainable bioprocesses for phosphorus recovery from waste. *Bioresour. Technol.* **2016**, *206*, 264−274.

(11) Bian, Y.; Chen, X.; Lu, L.; Liang, P.; Ren, Z. J. Concurrent Nitrogen and Phosphorus Recovery Using Flow-Electrode Capacitive Deionization. *ACS Sustainable Chem. Eng.* **2019**, *7*, 7844−7850.

(12) Gao, F.; Wang, L.; Wang, J.; Zhang, H.; Lin, S. Nutrient recovery from treated wastewater by a hybrid electrochemical sequence integrating bipolar membrane electrodialysis and membrane capacitive deionization. *Environ. Sci.: Water Res. Technol.* **2020**, *6*, 383−391.

(13) Huang, G.-H.; Chen, T.-C.; Hsu, S.-F.; Huang, Y.-H.; Chuang, S.-H. Capacitive deionization (CDI) for removal of phosphate from aqueous solution. *Desalin. Water Treat.* **2014**, *52*, 759−765.

(14) Hou, D.; Lu, L.; Sun, D.; Ge, Z.; Huang, X.; Cath, T. Y.; Ren, Z. J. Microbial electrochemical nutrient recovery in anaerobic osmotic membrane bioreactors. *Water Res.* **2017**, *114*, 181−188.
(15) Porada, S.; Zhao, R.; Van Der Wal, A.; Presser, V.; Biesheuvel, P. Review on the science and technology of water desalination by capacitive deionization. *Prog. Mater. Sci.* **2013**, *58*, 1388−1442.
(16) Guyes, E. N.; Malka, T.; Suss, M. E. Enhancing the ion-size-based selectivity of capacitive deionization electrodes. *Environ. Sci. Technol.* **2019**, *53*, 8447−8454.
(17) Huang, Z.; Lu, L.; Cai, Z.; Ren, Z. J. Individual and competitive removal of heavy metals using capacitive deionization. *J. Hazard. Mater.* **2016**, *302*, 323−331.
(18) Li, N.; An, J.; Wang, X.; Wang, H.; Lu, L.; Ren, Z. J. Resin-enhanced rolling activated carbon electrode for efficient capacitive deionization. *Desalination* **2017**, *419*, 20−28.
(19) Ma, J.; Liang, P.; Sun, X.; Zhang, H.; Bian, Y.; Yang, F.; Bai, J.; Gong, Q.; Huang, X. Energy recovery from the flow-electrode capacitive deionization. *J. Power Sources* **2019**, *421*, 50−55.
(20) Jeon, S.-i.; Park, H.-r.; Yeo, J.-g.; Yang, S.; Cho, C. H.; Han, M. H.; Kim, D. K. Desalination via a new membrane capacitive deionization process utilizing flow-electrodes. *Energy Environ. Sci.* **2013**, *6*, 1471−1475.
(21) Suss, M.; Porada, S.; Sun, X.; Biesheuvel, P.; Yoon, J.; Presser, V. Water desalination via capacitive deionization: what is it and what can we expect from it? *Energy Environ. Sci.* **2015**, *8*, 2296−2319.
(22) Moreno, D.; Hatzell, M. C. Influence of feed-electrode concentration differences in flow-electrode systems for capacitive deionization. *Ind. Eng. Chem. Res.* **2018**, *57*, 8802−8809.
(23) Ma, J.; Zhang, Y.; Collins, R. N.; Tsarev, S.; Aoyagi, N.; Kinsela, A. S.; Jones, A. M.; Waite, T. D. Flow-Electrode CDI Removes the Uncharged Ca−UO2−CO3 Ternary Complex from Brackish Potable Groundwater: Complex Dissociation, Transport, and Sorption. *Environ. Sci. Technol.* **2019**, *53*, 2739−2747.
(24) Luo, K.; Niu, Q.; Zhu, Y.; Song, B.; Zeng, G.; Tang, W.; Ye, S.; Zhang, J.; Duan, M.; Xing, W. Desalination behavior and performance of flow-electrode capacitive deionization under various operational modes. *Chem. Eng. J.* **2020**, No. 124051.
(25) He, C.; Ma, J.; Zhang, C.; Song, J.; Waite, T. D. Short-circuited closed-cycle operation of flow-electrode CDI for brackish water softening. *Environ. Sci. Technol.* **2018**, *52*, 9350−9360.
(26) Ge, Z.; Chen, X.; Huang, X.; Ren, Z. J. Capacitive deionization for nutrient recovery from wastewater with disinfection capability. *Environ. Sci.: Water Res. Technol.* **2018**, *4*, 33−39.
(27) Jiang, J.; Kim, D. I.; Dorji, P.; Phuntsho, S.; Hong, S.; Shon, H. K. Phosphorus removal mechanisms from domestic wastewater by membrane capacitive deionization and system optimization for enhanced phosphate removal. *Process Saf. Environ. Prot.* **2019**, *126*, 44−52.
(28) Choi, J.; Dorji, P.; Shon, H. K.; Hong, S. Applications of capacitive deionization: Desalination, softening, selective removal, and energy efficiency. *Desalination* **2019**, *449*, 118−130.
(29) Benjamin, M. M. *Water Chemistry*, 2nd ed.; Waveland Press: Long Grove, IL, 2014.
(30) Zhang, C.; Ma, J.; Song, J.; He, C.; Waite, T. D. Continuous ammonia recovery from wastewaters using an integrated capacitive flow electrode Membrane stripping system. *Environ. Sci. Technol.* **2018**, *52*, 14275−14285.
(31) Zhang, C.; Ma, J.; He, D.; Waite, T. D. Capacitive membrane stripping for ammonia recovery (CapAmm) from dilute wastewaters. *Environ. Sci. Technol. Lett.* **2018**, *5*, 43−49.
(32) Huang, X.; He, D.; Tang, W.; Kovalsky, P.; Waite, T. D. Investigation of pH-dependent phosphate removal from wastewaters by membrane capacitive deionization (MCDI). *Environ. Sci.: Water Res. Technol.* **2017**, *3*, 875−882.
(33) Zhang, J.; Tang, L.; Tang, W.; Zhong, Y.; Luo, K.; Duan, M.; Xing, W.; Liang, J. Removal and recovery of phosphorus from low-strength wastewaters by flow-electrode capacitive deionization. *Sep. Purif. Technol.* **2020**, *237*, No. 116322.
(34) Ma, J.; He, C.; He, D.; Zhang, C.; Waite, T. D. Analysis of capacitive and electrodialytic contributions to water desalination by flow-electrode CDI. *Water Res.* **2018**, *144*, 296−303.
(35) Lu, L.; Huang, Z.; Rau, G. H.; Ren, Z. J. Microbial electrolytic carbon capture for carbon negative and energy positive wastewater treatment. *Environ. Sci. Technol.* **2015**, *49*, 8193−8201.
(36) Bian, Y.; Ge, Z.; Albano, C.; Lobo, F. L.; Ren, Z. J. Oily bilge water treatment using DC/AC powered electrocoagulation. *Environ. Sci.: Water Res. Technol.* **2019**, *5*, 1654−1660.
(37) Wang, L.; Lin, S. Mechanism of selective ion removal in membrane capacitive deionization for water softening. *Environ. Sci. Technol.* **2019**, *53*, 5797−5804.
(38) Moreno, D.; Bootwala, Y.; Tsai, W.-Y.; Gao, Q.; Shen, F.; Balke, N.; Hatzell, K. B.; Hatzell, M. C. In Situ Electrochemical Dilatometry of Phosphate Anion Electrosorption. *Environ. Sci. Technol. Lett.* **2018**, *5*, 745−749.
(39) Yu, J.; Jo, K.; Kim, T.; Lee, J.; Yoon, J. Temporal and spatial distribution of pH in flow-mode capacitive deionization and membrane capacitive deionization. *Desalination* **2018**, *439*, 188−195.
(40) Zhao, R.; Biesheuvel, P.; Van der Wal, A. Energy consumption and constant current operation in membrane capacitive deionization. *Energy Environ. Sci.* **2012**, *5*, 9520−9527.
(41) Chingombe, P.; Saha, B.; Wakeman, R. Surface modification and characterisation of a coal-based activated carbon. *Carbon* **2005**, *43*, 3132−3143.
(42) Dai, M. The effect of zeta potential of activated carbon on the adsorption of dyes from aqueous solution: I. The adsorption of cationic dyes: methyl green and methyl violet. *J. Colloid Interface Sci.* **1994**, *164*, 223−228.
(43) Li, F.; Yuasa, A.; Ebie, K.; Azuma, Y. Microcolumn test and model analysis of activated carbon adsorption of dissolved organic matter after precoagulation: effects of pH and pore size distribution. *J. Colloid Interface Sci.* **2003**, *262*, 331−341.
(44) Song, X.; Liu, H.; Cheng, L.; Qu, Y. Surface modification of coconut-based activated carbon by liquid-phase oxidation and its effects on lead ion adsorption. *Desalination* **2010**, *255*, 78−83.
(45) He, D.; Wong, C. E.; Tang, W.; Kovalsky, P.; Waite, T. D. Faradaic reactions in water desalination by batch-mode capacitive deionization. *Environ. Sci. Technol. Lett.* **2016**, *3*, 222−226.
(46) Hemmatifar, A.; Oyarzun, D. I.; Palko, J. W.; Hawks, S. A.; Stadermann, M.; Santiago, J. G. Equilibria model for pH variations and ion adsorption in capacitive deionization electrodes. *Water Res.* **2017**, *122*, 387−397.
(47) Dykstra, J. E.; Keesman, K.; Biesheuvel, P.; Van der Wal, A. Theory of pH changes in water desalination by capacitive deionization. *Water Res.* **2017**, *119*, 178−186.
(48) Lee, J.-H.; Bae, W.-S.; Choi, J.-H. Electrode reactions and adsorption/desorption performance related to the applied potential in a capacitive deionization process. *Desalination* **2010**, *258*, 159−163.

https://dx.doi.org/10.1021/acs.est.0c01836
Environ. Sci. Technol. 2020, 54, 9116−9123